A SPECTROMETRIC INVESTIGATION OF AN ELECTRODELESS DISCHARGE

By
KYNRIC MARTIN PELL

A DISSERTATION PRESENTED TO THE GRADUATE COUNCIL OF
THE UNIVERSITY OF FLORIDA
IN PARTIAL FULFILLMENT OF THE REQUIREMENTS FOR THE
DEGREE OF DOCTOR OF PHILOSOPHY

UNIVERSITY OF FLORIDA
August, 1967

to my wife

and

parents

ACKNOWLEDGEMENTS

The author wishes to acknowledge the assistance provided by the members of his supervisory committee throughout the period of graduate study. He especially wishes to express his gratitude to his chairman Dr. M. H. Clarkson, whose guidance and encouragement made this dissertation possible.

A special acknowledgement is due to the National Aeronautics and Space Administration who supported this study under Grant No. NsG-542.

The author wishes to thank Mr. James Moorhead for his assistance in data reduction and preparation of the figures.

Finally, the author wishes to thank his wife, Ann, for her painstaking care in the preparation of this dissertation and her patience throughout the period of study.

TABLE OF CONTENTS

		Page
ACKNOWLEDGEMENTS		iii
LIST OF TABLES		vi
LIST OF FIGURES		vii
LIST OF SYMBOLS		ix
ABSTRACT		xi
CHAPTER		
I	INTRODUCTION	1
II	PLASMA MODELS Discussion Thermal Plasma Corona Plasma Collision-Radiative Plasma (Semi-Corona) Regions of Validity for Local Thermodynamic Equilibrium Regions of Validity for Corona Equilibrium Regions of Validity for Collisional-Radiative or Semi-Corona Domain	4
III	THE MODEL OF THE ARGON PLASMA	15
IV	RADIATION FROM A FINITE SOURCE External Optical System Irradiance of the Image of an Extended Source Experimental Verification of the Law of Irradiance for an Extended Source Spatial Resolution of Cylindrically Symmetric Sources	20
V	EXPERIMENTAL PROCEDURES Experimental Apparatus Power Supply Vacuum System Spectroscopic Instrumentation Data Reduction	25

TABLE OF CONTENTS (Continued)

Page

VI RESULTS AND CONCLUSIONS 30

FIGURES 1 - 30 33-64

APPENDIX
NUMERICAL INVERSION OF ABEL'S EQUATION . . . 66

LIST OF REFERENCES 68

BIOGRAPHICAL SKETCH 70

LIST OF TABLES

Table | Page

1. Results..... 65

LIST OF FIGURES

Figure		Page
1.	Temperature Distribution	33
2.	Domains of Validity for an Optically Thin Argon Plasma	34
3.	Ratio of Neutral Atoms to Singly Ionized Ions for Argon	35
4.	Saha Equation Correction Factor for Argon Atoms	36
5.	Collision Limit for Argon Atoms	37
6.	Collision Limit for Argon Ions	38
7.	Ratio of Excited Neutrals to Excited Ions	39
8.	Emission Line Intensity Ratio	40
9.	Law of Irradiance	41
10.	Experimental Verification of the Law of Irradiance	42
11.	Spectral Intensity Calibration	43
12.	Geometry of the Source	44
13.	Plasma Chamber	46
14.	Instrumentation	48
15.	Integrated Intensity Profile 4806 Å	49
16.	Integrated Intensity Profile 4347 Å	50
17.	Integrated Intensity Profile 7503 Å	51

LIST OF FIGURES (Continued)

Figure		Page
18.	Integrated Intensity Profile 7514 Å.....	52
19.	Radial Intensity Distribution 4806 Å.....	53
20.	Radial Intensity Distribution 4347 Å.....	54
21.	Radial Intensity Distribution 7503 Å.....	55
22.	Radial Intensity Distribution 7514 Å.....	56
23.	Radial Temperature Distribution Run 13.....	57
24.	Radial Temperature Distribution Run 14.....	58
25.	Radial Temperature Distribution Run 15.....	59
26.	Radial Temperature Distribution Run 16.....	60
27.	Radial Temperature Distribution Run 17.....	61
28.	Radial Temperature Distribution Run 18.....	62
29.	Radial Temperature Distribution Run 19.....	63
30.	Peak Temperature as a Function of Input Power.....	64

LIST OF SYMBOLS

N	-	Total number density of atoms
$N^{(Z)}$	-	Total number density of ions in ionization stage Z
$N_p^{(Z)}$	-	Number density of atoms in excited state p and ionization stage Z (Z = 1 for atoms)
N_e	-	Number density of electrons
g_p	-	Statistical weight of state p
k	-	Boltzmann constant
T	-	Temperature
$U(T)$	-	Partition function
$E_p^{(Z)}$	-	Excitation energy of state p in ionization stage Z
α_o	-	First Bohr radius
E_H	-	Ionization energy of hydrogen
$E^{(Z)}$	-	Ionization energy of ion in stage Z
$\Delta E_\infty^{(Z)}$	-	Reduced ionization potential
p	-	Pressure
e	-	Electron
$h\nu$	-	Photon
S	-	Collisional ionization rate

α - Radiative recombination rate

ξ - Number of equivalent electrons

X - Collision excitation function

A_p - Total transition probability for the state p

A_{pq} - Transition probability for transitions from p to q

β - Collisional recombination coefficient

γ_{nm} - Correction factor

ν - Frequency

I - Intensity

H - Irradiance

J - Radiant intensity

H_λ - Spectral irradiance

N_λ - Spectral radiance

μ - Index of refraction

m - Magnification

λ - Wave length

Abstract of Dissertation Presented to the Graduate Council in Partial Fulfillment of the Requirements for the Degree of Doctor of Philosophy

A SPECTROMETRIC INVESTIGATION OF AN ELECTRODELESS DISCHARGE

By

Kynric Martin Pell

August, 1967

Chairman: Dr. M. H. Clarkson

Major Department: Aerospace Engineering

This dissertation is concerned with the experimental determination of the electron temperature distribution in a nonequilibrium, low pressure, electrodeless discharge. In view of the lack of excitation function data for complex atoms, such as argon which was used in this study, an approximate semi-corona model was used. The temperature dependence of excited state population densities for neutral atoms and singly ionized ions predicted by the approximate model was used to obtain a relationship between the intensity ratio of two emission lines and the temperature.

Integrated intensity distribution data were inverted numerically to obtain the radial dependence of the intensity.

Ratios of the intensity of an ion emission line and an atom emission line at 25 radial locations in the plasma were used to obtain the temperature distributions.

Maximum temperatures, found on the axis of symmetry, ranged from 1.24 to 1.54 ev. for a range of operating pressures from 50 to 1000 microns of mercury. The radial dependence of the temperature was found to be quite weak. The temperature decreases approximately 15% over a region equal to 2/3 of the radius of the plasma.

CHAPTER I

INTRODUCTION

An electrodeless discharge is a plasma which is formed by the excitation of a gas by either c.w. or pulsed radio frequency (r.f.) fields. The discovery of the electrodeless discharge is usually attributed to Hittorf,[1] in the year 1884. For over 40 years following its discovery, a controversy raged regarding the nature of the discharge. Hittorf[1] and J. J. Thomson[2] contended that the discharge was due to electromagnetic induction. Townsend and Donaldson,[3] as well as Lehrmann,[4] among others, maintained that the discharge was due to the large potential difference between the ends of the current carrying coil. In 1929, K. A. MacKinnon[5] described two different modes of operation he found in the electrodeless discharge which were primarily dependent upon working gas pressure, coil configuration, and coil current. He found that Thomson's work was confined to a small range of pressures involving ring-type discharges exclusively. MacKinnon concluded that ring discharges were, in fact, due to electromagnetic fields. On the other hand Townsend and Donaldson treated a glow discharge over a wide range of pressures and apparently failed to realize the difference between the ring and glow modes of operation. MacKinnon concluded that the glow mode of operation was either largely, or entirely, due to electrostatic excitation.

This resolved the controversy and it was 1960 before Reed[6] applied electromagnetic induction to a flowing gas at atmospheric pressure to create an electrodeless plasma torch. Quantitative temperature determinations made by Reed, using spectrographic techniques and the Fowler-Milne method, resulted in the temperature distribution shown in Figure 1. In 1963 Reed[7] investigated static plasmas of several gases over a range of pressures from .005 mm of mercury to atmospheric pressure using spectroscopic techniques. He observed two different modes of operation which were reflected in different spectra obtained at various pressures and plate powers. However he did not make further quantitative temperature predictions. Pell,[8] in 1963, utilized a stagnation point heat transfer probe to measure the temperature distribution in an atmospheric pressure plasma torch yielding a significantly different temperature distribution than obtained by Reed. Spectroscopic work by Gold'farb and Dresvin,[9] Pettit,[10] and Johnston[11] among others has confirmed the lower temperatures obtained by Pell for the atmospheric pressure plasma torch. A typical temperature distribution for such a torch is shown in Figure 1.

At pressures below atmospheric, probe studies have been made by Clarkson, et al.,[12] and Keefer, et al.[13] Some spectrometric measurements were made by Porter[14] wherein a corona model of the plasma was used in the interpretation of the data. Sovie[15, 16] has applied both probe and spectrometric techniques to a flowing helium plasma in the pressure range of 0 to 100 microns obtaining reasonable agreement between the two techniques.

The problem associated with any spectrometric diagnostic

attempt on the low pressure discharge is that it is difficult to determine the number density of atoms or ions in the various excited states. Sovie's success with helium was dependent on the hydrogenic approximation and the fact that excitation cross-sections for such ions have been calculated and experimentally verified.

The problem addressed in this work is the temperature determination in a low pressure (50 to 1000 microns) argon electrodeless discharge. A semi-corona model of the plasma is used in this study. A functionally simple semi-corona ionization equation described by Oertel[17] is applied to an argon electrodeless discharge. Non-equilibrium, steady-state populations of the various excited states of the atom and ion predicted by Oertel's method are used to obtain a relationship between the intensity ratio of two emission lines and the electron temperature.

Integrated spectrometric intensity data for four argon emission lines are inverted using Abel's equation to obtain radial intensity distributions in the discharge. These radial distributions are used to obtain local values of I_{7503}/I_{4806} and I_{7514}/I_{4347} from which temperature distributions are obtained.

Temperatures were obtained for a range of input power levels from 220 to 740 watts in the pressure range from 50 to 1000 microns. These results are presented in Table I.

CHAPTER II

PLASMA MODELS

Discussion

The basic problem associated with any spectroscopic technique is relating the intensity of radiation to the plasma properties.

There are currently three microscopic models of a plasma in use for the interpretation of spectrometric data. These models which are termed thermal, corona, and semi-corona (or collisional-radiative) are assumed to apply to plasmas in different states. The rate processes for populating and depopulating the various excited states in the plasma are proportional to the number density of electrons N_e and the electron temperature T_e. Population by photon induced excitations or ionizations is usually neglected on the assumption, or experimental verification, that the plasma is optically thin. The domains of applicability of the various models can be represented on a graph of N_e vs T_e for any particular type of gas and this has been done in Figure 2 for argon. The criteria used in constructing such a graph are presented in the following sub-sections. A description of each of the three models follows.

Thermal Plasma

Thermal plasmas are those in which the population of excited states is in accord with the Boltzmann distribution.

That is

$$\frac{N_p}{N} = \frac{g_p \exp\left[-E_p/kT\right]}{U(T)} \tag{2.1}$$

where

$$U(T) = \sum_p g_p \exp\left[-E_p/kT\right] \tag{2.2}$$

N = total number density of atoms in all excited states and the ground state.

N_p = number density of atoms in excited state p.

g_p = statistical weight of state p.

E_p = excitation energy of state p.

k = Boltzmann constant.

T = Temperature.

U(T) = Partition function.

For complete thermodynamic equilibrium to exist, detailed balancing is required. This condition is rarely found in laboratory plasmas. However, the concept of local thermodynamic equilibrium (LTE) may be applicable when detailed balancing is not satisfied.

Whenever local thermodynamic equilibrium exists, the densities in specific quantum states are those existing in a system in complete thermodynamic equilibrium which has the same mass (total) density, temperature, and chemical composition as the LTE system. The temperature referred to is that of the specie dominating the reaction rates. In general this is the electron.

The distribution of excited states in LTE is given by

$$\frac{N_p}{N} = \frac{g_p \exp\left[-E_p / kT_e\right]}{U(T_e)} \tag{2.3}$$

where T_e is the electron temperature. It is not necessary for the ions, nor the atoms, to have the same temperature as the electrons. However, $T_e \geq T_g$ and T_i.

In an LTE plasma ionization equilibrium is expressed by the Saha equation

$$\frac{N^{Z+1} N_e}{N^Z} = \frac{2}{a_o^3} \frac{U^{Z+1}}{U^Z} \left[\frac{kT_e}{4\pi E_H}\right]^{3/2} \exp\left[\frac{-(E_\infty^Z - \Delta E_\infty^Z)}{kT_e}\right] \tag{2.4}$$

where

N^Z = number density of ions in ionization stage Z. (Z = 1 for atoms)

N_e = number density of electrons.

a_o = first Bohr radius.

E_H = ionization energy of hydrogen.

ΔE_∞^Z = reduced ionization potential.

The hydrostatic pressure of the gas is given by Dalton's law of partial pressures

$$p = \sum_i N_i \, k T_i \tag{2.5}$$

where the i includes all species and stages of ionization. The additional requirement of quasi-neutrality

$$N_e = \sum_i (Z_i - 1) N_i \tag{2.6}$$

where i refers to stage of ionization, completes a set of equations which can be used to determine the composition of an LTE gas.

For this model to apply to a gas, the electron density must be sufficiently large to insure that the population of all states is dictated by electron collisional excitation and de-excitation rates. Radiative losses are assumed to be negligibly small.

Corona Plasma

The most extreme departure from LTE is described by the corona model which has been proposed as a model of the solar corona. (See, e.g. reference 18). In LTE the process of collisional ionization is balanced by three-body recombination

$$e + N^z \rightleftharpoons N^{z+1} + e + e \tag{2.7}$$

As the number density of electrons decreases, the process of radiative recombination becomes large compared to the three-body recombination process, i.e.

$$e + N^{z+1} \longrightarrow N^z + h\nu \tag{2.8}$$

In this model, it is assumed that the electrons have a Maxwellian distribution of velocities and that the mean energy of the ions and atoms is equal to, or less than,

that of the electrons. In addition it is assumed that the population of all excited states is negligible compared to the ground state. An equation relating the collisional ionization rate to the radiative recombination rate may now be written as

$$Ne\ N_g^z\ S(T_e,z,g) = Ne\ N_g^{z+1} \alpha(T_e,z+1,g) \tag{2.9}$$

or

$$\frac{N_g^z}{N_g^{z+1}} = \frac{\alpha(T_e,z+1,g)}{S(T_e,z,g)} \tag{2.10}$$

Results of detailed calculations of S by Burgess, which were based on the Coulomb-Born approximation, are given by McWhirter.[18] Also, a general formula for α is given by McWhirter.[18] The expressions for S and α may be used to write an ionization balance equation of the form

$$\frac{N_g^z}{N_g^{z+1}} = \frac{1.18 \times 10^{-4} Z^2 (E_g^z)^{7/4}}{\xi T_e^{3/4}} \exp\left[\frac{E_g^z}{kT_e}\right] \tag{2.11}$$

where ξ is the number of equivalent electrons.

The population of the pth excited state may be related to the ground state by the expression

$$\frac{N_p^z}{N_g^z} = \frac{Ne\ X(z,q,p)}{A(z,p)} \tag{2.12}$$

where $X(Z,g,p)$ is the collision excitation function for the temperature T_e and $A(Z,p)$, sometimes written as A_p^Z, is the total transition probability for the state p.

Application of this model requires that the electron number density be sufficiently low so that the collisional de-excitation term can be neglected in the ionization balance equation (2.9).

Collision-Radiative Plasma (Semi-Corona)

When the electron density is too low to insure LTE and too high to apply the corona model, the electronic state of the atoms and ions in the plasma must be determined from a system of rate equations. That is, the steady state population of an excited level is a function of both radiative and collisional processes. The assumptions required to set up such a system of equations are listed below:[18]

(1) The free electrons must have a Maxwellian distribution

(2) Ionization is by electron collision from the bound levels of the lower stage of ionization and is only partially balanced by three-body recombination

$$N_p^z + e \rightleftharpoons N_g^{z+1} + e + e \qquad (2.13)$$

(3) Transitions between bound levels may be induced by electron collisions

$$N_p^z + e \rightleftharpoons N_g^z + e \qquad (2.14)$$

(4) Radiation is emitted when an electron in a higher bound state p, spontaneously decays to a lower state g and when a free electron makes a transition to a bound level

$$N_p^Z \rightarrow N_g^Z + h\nu_{pg} \tag{2.15}$$

$$N_g^{Z+1} + e \rightarrow N_p^Z + h\nu \tag{2.16}$$

Using the above assumptions the equations describing the rates at which the various excited states are populated may be written

$$\begin{aligned}\frac{dN_p^Z}{dt} = & -N_p^Z\{N_e S(T_e,Z,p) + N_e \sum_{g\neq p} X(T_e,Z,p,g) \\ & + \sum_{g<p} A(Z,pg)\} + N_e \sum_{g\neq p} N(Z,p) X(T_e,Z,g,p) \\ & + \sum_{g>p} N_p^Z A(Z,g,p) + N_e N_g^{Z+1}\{N_e \beta(T_e,Z+1,p) \\ & + \alpha(T_e,Z+1,p)\}\end{aligned} \tag{2.17}$$

where $\beta(T_e, Z+1, p)$ is the collisional recombination coefficient.

In general the solution of a set of equations, typified by (2.17) for all states of the atoms and ions in a plasma is not possible even when the number of states is reduced to a finite number by the reduced ionization potential. The problem is not the number of equations but the lack of rate coefficients $S(T_e,Z,p)$, $A(Z,p,g)$, etc. for complex atoms or ions. Detailed calculations for

hydrogen and hydrogen-like ions have been made by several researchers[17] using several assumptions in addition to the four given above.

Oertel[17] has proposed an approximation for the semi-corona model which assumes that the electronic excitation of the atoms or ions can be described by two different Boltzmann distributions while the ionization equilibrium is given by a corrected Saha equation.

If the electron number density in an arbitrary plasma is reduced, departures from LTE will start at the lowest energy levels of the atom or ion. For any steady state in the collision-radiative or semi-corona domain, the ratio of population densities of the higher states are given by the Boltzmann relation

$$\frac{N_n^z}{N_m^z} = \frac{g_n^z}{g_m^z} \exp\left[\frac{-(E_n^z - E_m^z)}{kT_e}\right] \tag{2.18}$$

That is, the higher states are in LTE. For the lower states, a correction factor τ_{nm} is introduced so that (2.18) becomes

$$\frac{N_n^z}{N_m^z} = \frac{\tau_{nm}\, g_n^z}{g_m^z} \exp\left[\frac{-(E_n^z - E_m^z)}{kT_e}\right] \tag{2.19}$$

τ_{nm} is obtained by requiring (2.19) to predict the same ratio as the corona model. An expression for τ_{nm} based on hydrogen and hydrogenic ions is obtained by Oertel.[17] However, a simpler form is given by Schneider and Oertel[19] which shows better agreement with detailed calculations by Bates, et al.[20]

This expression for τ_{nm} is

$$\tau_{nm} \equiv \tau' = 18\xi\, Ne \left(\frac{\alpha_o}{\alpha}\right)^3 \left[\frac{E_H}{E_\infty^Z - \mathcal{E}_o}\right]^3 \left[\frac{E_H}{E_\infty^Z}\right]^{1/2}, \text{ for } \tau' < 1$$

$$\tau_{nm} = 1, \text{ for } \tau' \geq 1$$

(2.20)

where α = fine structure constant, and $\mathcal{E}_o$ = collision limit to be defined later. The modified Saha equation used in this approximation is

$$\frac{N^{Z+1} Ne}{N^Z} = \frac{\tau\, 2\, U^{Z+1}}{\alpha_o^3\, U^Z} \left[\frac{kT_e}{4\pi E_H}\right]^{3/2} \exp\left[\frac{-(E_\infty^Z - \Delta E_\infty^Z)}{kT_e}\right]$$

(2.21)

The collision limit is a state with principal quantum number n' where the excitation level of n' is

$$E(n') = E_\infty^Z - \mathcal{E}_o$$

(2.22)

In general n' is nonintegral. However, there is no necessity to associate n' with a particular energy level of the atom or ion since one only desires to know the regions of applicability of the various Boltzmann equations.

The state n' is determined by equating the collisional excitation rates to the radiative decay rates and solving for the energy at which this situation will occur. The form of $\mathcal{E}_o$, as defined in (2.22), is given by Schneider and Oertel[19] as

$$\mathcal{E}_o = E_H \left[\frac{3}{4} Ne \left(\frac{\alpha_o}{\alpha}\right)^3 \left(\frac{E_H}{E_\infty^Z}\right)^2 Z^7\right]^{2/9} \qquad (2.23)$$

The reduced ionization potential ΔE_∞^Z is given by Griem[21] as

$$\Delta E_\infty^Z = 2(Z+1) E_H \left[\frac{8\pi E_H a_0^3 (N_e + Z_j^2 N_j)}{kT_e} \right]^{1/2} \quad (2.24)$$

However, a much simpler form proposed by Schneider[22] has been used here, namely

$$\Delta E_\infty^Z = 0.67 \times 10^{-6} (N_e)^{1/2} + 0.37 \times 10^{-7} \left(\frac{N_e}{T} \right)^{1/2} \quad (2.25)$$

Regions of Validity for Local Thermodynamic Equilibrium

In order that a stationary homogeneous plasma be in local thermodynamic equilibrium, a minimum electron density requirement must be imposed to insure that radiative transitions between two states are less than 10% as frequent as de-excitations by electron collisions. Since radiative rates tend to decrease with higher levels of excitation and whereas collisional rates tend to increase, LTE is more probable for higher excited states if the electron number density is too low to permit complete LTE. Schneider and Oertel[19] give a minimum electron density to insure LTE between excited states m, located above a limiting state n', and the continuum for a non-hydrogenic atom in the form

$$N_e \geq 1.9 \times 10^{18} \frac{Z^{-5/2}}{\left[\frac{E_\infty^Z - E_m^Z}{E_H} \right]^{17/4}} \left[\frac{kT_e}{E_H} \right]^{1/2}$$

This condition was used to set the lower boundary of the LTE region on Figure 2. If the plasma is inhomogeneous, then the mean free path of atoms between equilibrating

collisions must be short compared to the distance over which the plasma conditions change appreciably. Further discussion of this criterion may be found in reference 21.

Regions of Validity for Corona Equilibrium

The corona domain may be defined as that domain where the rate coefficients α_t and S_t for the thermal (higher excitation) levels are much less than the corresponding coefficients α and S for the continuum. This definition has been used by Wilson[23] to establish an upper limit on the electron density given by

$$N_e \leq 1.5 \times 10^{10} (E_\infty^z)^{-1/2} (kT_e)^4$$

This is the condition used in the graph of Figure 2 in order to establish the corona limit.

Regions of Validity for Collisional-Radiative or Semi-Corona Domain

As may be seen from Figure 2, the region between the two limits defined above is the collisional-radiative domain.

CHAPTER III

THE MODEL OF THE ARGON PLASMA

Probe data taken by Keefer, et al., indicate that the electrodeless discharge in argon operates at an electron temperature in excess of 1.0 volt with a maximum electron number density on the axis of approximately 5.0×10^{12} cm^{-3}. In view of the discussion in Chapter II, it appears that the appropriate microscopic model for the low pressure electrodeless discharge is the semi-corona model. The lack of either experimental or theoretical cross-sections, excitation functions, and other atomic parameters for complex atoms, such as argon, make the solution of the rate equations a practical impossibility. Two approximate forms for the semi-corona region are available. The approach due to Oertel described in Chapter II is used in the following analysis because of its simplicity. A considerably more detailed approach is given by Griem.[21] The development of Oertel's approach for an argon plasma follows.

The intensity ratio of two emission lines in a steady state plasma is given by the equation

$$\frac{I^{(1)}}{I^{(2)}} = \frac{\nu_1 A_{pq} \int_0^L N_q^{(1)}(x)\, dx}{\nu_2 A_{mn} \int_0^L N_n^{(2)} x\, dx} \qquad (3.1)$$

where $I^{(1)}$ is the intensity of spectral line (1) having frequency ν_1 and originating from transitions between level q and level p. A_{pq} is the transition probability associated with the levels p and q. The integration is over the extent of the plasma along the line of sight of the detector. If the experimental data can be unfolded so that local intensity ratios can be obtained, the integration may be eliminated and equation (3.1) may be written

$$\frac{I^{(1)}}{I^{(2)}} = \frac{\nu_1 A_{pq} N_q^{(1)}}{\nu_2 A_{mn} N_n^{(2)}} \qquad (3.2)$$

where the intensity ratio is a function of radial location. The problem of unfolding the intensity data is discussed in Chapter IV. In general, the ratio $N_q^{(1)} / N_n^{(2)}$ is a strong function of the temperature if the excited states q and n are in different ionization stages. Using a semi-corona model, the ratio $N_q^{(1)} / N_n^{(2)}$ will be related to the temperature so that an intensity ratio measurement can be used to determine the temperature.

The number density in a particular excited state n, of ionization stage (Z), can be related to the total number density of the element by the equation

$$N_n^{(Z)} = \frac{N_n^{(Z)}}{N^{(Z)}} \frac{N^{(Z)}}{N} N \qquad (3.3)$$

For a system in equilibrium

$$\frac{N_n^{(Z)}}{N^{(Z)}} = \frac{N_n^{(Z)}}{N_g^{(Z)}} \frac{g_g^{(Z)}}{U^{(Z)}(kT_e)}$$

(3.4)

where g refers to the ground state. The usual assumption made in analyses of this type is that the partition function may be replaced by its first term, so that

$$\frac{N_n^{(Z)}}{N^{(Z)}} = \frac{N_n^{(Z)}}{N_g^{(Z)}}$$

(3.5)

To take into account nonequilibrium populations a correction factor τ_{ng} is introduced into the Boltzmann relation which gives

$$\frac{N_n^{(Z)}}{N_g^{(Z)}} = \frac{\tau_{ng}\, g_n^{(Z)}}{g_g^{(Z)}} \exp\left[-\frac{(E_n^{(Z)} - E_g^{(Z)})}{kT_e}\right]$$

(3.6)

Equation (3.3) may now be written in the form

$$N_n^{(Z)} = \frac{\tau_{ng}\, g_n^{(Z)}}{g_g^{(Z)}} \exp\left[-\frac{(E_n^{(Z)} - E_g^{(Z)})}{kT_e}\right] \frac{N^{(Z)} N}{N}$$

(3.7)

The ratio $N_n^{(Z+1)} / N_p^{(Z)}$ may be written in the form

$$\frac{N_n^{(Z+1)}}{N_p^{(Z)}} = \frac{\tau_{ng}}{\tau_{pg}} \frac{g_n^{(Z+1)}}{g_g^{(Z+1)}} \frac{g_g^{(Z)}}{g_p^{(Z)}} \exp\left[\frac{-(E_n^{(Z)} - E_g^{(Z)}) + E_p^{(Z+1)} - E_g^{(Z+1)}}{kT_e}\right] \frac{N^{(Z+1)}}{N^{(Z)}}$$

(3.8)

The ratio of $N^{(Z+1)}/N^{(Z)}$ is given by the corrected Saha equation (2.21). Figure 3 shows the dependence of $N^{(2)}/N^{(1)}$ on temperature for argon at electron densities of 10^{10}, 10^{12}, and 10^{14} cm^{-3}. The values of the Saha correction factor, γ, and the collision limit, $\mathcal{E}_o$, required to construct Figure 3 were determined using equations (2.20) and (2.23). The results are presented in Figures 4 and 5, respectively. All of the emission lines used in this study originated from levels lying below the collision limit, n'. Therefore, the form of the Boltzmann equation used in determining the populations of the appropriate upper states of the atoms and ions includes the correction factor γ. For the atoms, this correction factor is the same as that previously used in the Saha equation. A similar graph was made for the ions. However, it is not presented here. Using equation (3.8), the correction factor $\gamma_{ng}^{(2)}$, the correction factor $\gamma_{pq}^{(1)}$, and the ratio $N^{(2)}/N^{(1)}$, a graph of $N_n^{(1)}/N_p^{(2)}$, where n corresponds to the 107054.32 cm^{-1} level of neutral argon, (ArI), and p corresponds to the 157234.93 cm^{-1} level of singly ionized argon, (ArII), is plotted for various electron densities on Figure 7. A similar calculation for the ArI level 108722.67 cm^{-1} and the ArII level 155044.07 cm^{-1} gives the same result. Thus, Figure 7 represents the ratio $N_n^{(1)}/N_p^{(2)}$ for the two population ratios used in this study.

Using equation (3.2), the intensity ratios I_{7503}/I_{4806} and I_{7514}/I_{4347} were plotted as a function of temperature in Figure 8 for an assumed number density of 10^{12} electrons cm^{-3}. A variation in electron density of 10^4 cm^{-3}

results in a temperature change of .15 ev. or approximately 10% for the temperatures determined in this investigation. The transition probabilities used in this study were those given by Olsen.[24]

CHAPTER IV

RADIATION FROM A FINITE SOURCE

External Optical System

To make relative or absolute intensity measurements on an inhomogeneous finite radiating source, an external optical system is usually used to image the source on the entrance slit of a spectrometer. Since the source is three dimensional, the question arises as to where the optical system should focus in the source and indeed how does one interpret the data since they are obtained from an integrated intensity over the source in the field of view of the optical system. An analytical treatment of the radiation from a finite source is considered in the following section which is then followed by a description of an experimental verification of the results.

Irradiance of the Image of an Extended Source

Consider the system shown in Figure 9 where the source is of radiance N and its image is of radiance N'. We wish to find the irradiance H at any point in the image space. Let $d\sigma$ be an element of area at a distance X from the source. Its image is $d\sigma'$. Consider a pencil of rays of radiant intensity, J, included in the angle $d\theta$ at an angle θ from the optical axis. If Lambert's cosine law is obeyed, then the irradiance dH at $d\sigma$ is given by

$$dH = \frac{dJ \cos\theta}{X^2 \sec^2\theta} \tag{4.1}$$

But $$dJ = 2\pi r\, dr\, N \cos\theta \tag{4.2}$$

so that $$dH = \frac{2\pi r\, dr\, N \cos^2\theta}{X^2 \sec^2\theta}$$

Note that $r = X \tan\theta$ and that $dr = X \sec^2\theta \cdot d\theta$

Therefore $$H = \int_0^\theta 2\pi N \sin\theta \cos\theta\, d\theta$$

$$= 2\pi N \int_0^\theta \sin\theta \cos\theta\, d\theta$$

$$= \pi N \sin^2\theta \tag{4.3}$$

The Abbe sine condition gives the magnification as

$$m = \frac{\ell'}{\ell} = \frac{\mu \sin\theta}{\mu' \sin\theta'}$$

Squaring and rearranging gives

$$\sin^2\theta = m^2 \left(\frac{\mu'}{\mu}\right)^2 \sin^2\theta' \tag{4.4}$$

Conservation of energy in the optical system yields

$$H = m^2 H' \tag{4.5}$$

Substituting (4.4) and (4.5) into (4.3) gives

$$m^2 H' = \pi N m^2 \left(\frac{\mu'}{\mu}\right)^2 \sin^2\theta' \tag{4.6}$$

For source and receiver planes both in air, $\mu = \mu'$ and the Law of Irradiance may be written

$$H' = \pi N \sin^2 \theta' \tag{4.7}$$

This result is independent of the location of $d\sigma'$ so that if we assume that this plane coincides with the plane of the entrance slit we see that the irradiance of the entrance slit by any surface in the source is given by

$$H' = \pi N \sin^2 \theta' \tag{4.8}$$

If it is not desired to resolve the intensity distribution spatially, it is not necessary to use an imaging optical system for the external optics.

Experimental Verification of the Law of Irradiance for an Extended Source

A glow discharge tube was mounted on a movable stand which was attached to an optical bench. The discharge tube could be moved up and down (scanned across its diameter) in .01 mm increments. An image of the discharge tube was focused on a slit by a single lens. A photomultiplier located behind the slit recorded the total intensity of radiation from the field of view of the optical system. An adjustable stop was used to vary the f number of the optical system. For a range of f numbers from 9 to 36 and an out of focus condition of $\pm$ 10% of twice the focal length of the lens the intensity distribution for the discharge tube as recorded by the photomultiplier remained essentially unchanged. The deviations in the intensity distributions for the various f numbers and focusing conditions was less than 1% as shown in Figure 10.

Spatial Resolution of Cylindrically Symmetric Sources

It may be seen from the law of irradiance that the amount of light entering the entrance slit of the spectrometer from an extended uniform source is independent of the position of the source on the optical axis of the system. If the source is in focus within a reasonable experimental error and the plasma properties can be considered constant across a plane perpendicular to the optical axis which is bounded by the field of view of the optical system, the irradiance of the entrance slit is given by

$$H = \pi \sin^2\theta' \int_0^L N(X)\, dX \tag{4.9}$$

where the integration is along the line of sight (optical axis) through the plasma. For spectroscopic work one is interested in relating spectral irradiance, that is power per unit wavelength interval per cm^{-2} incident on the entrance slit, to the spectral radiance of the source, i.e.

$$H_\lambda = \pi \sin^2\theta' \int_0^L N_\lambda(X)\, dX \tag{4.10}$$

The quantity measured by the spectrometer is $H_\lambda \quad K_i$, where K_i is an experimental constant which depends on the system response of the spectrometer and the geometry of the external optical system. Assuming the geometry of the system is held constant, only the wavelength dependence of K_i must be taken into account for intensity ratio techniques.

The system response was calibrated using a tungsten ribbon-filament standard of spectral radiance. Figure 11

contains the results and the system response correction factors used in the experimental work. Applying these corrections to the raw data, values of $H_\lambda \gamma'$, are obtained where γ' is a single valued, geometry dependent constant.

There remains the problem of relating $H_\lambda \gamma'$ to $N_\lambda(X)$. For sources possessing cylindrical symmetry

$$\gamma' H_\lambda(y) = 2 \int_{r=y}^{R} \frac{\gamma' N(r) r \, dr}{(r^2 - y^2)^{1/2}} \tag{4.11}$$

Figure 12 illustrates the geometric relationships. Following the method outlined by Pearce,[25] a numerical scheme for solving equation (4.11) for $\gamma' N_\lambda(r)$ was developed for the computer. The source was assumed to be composed of 25 concentric rings having constant plasma properties. The code developed for this work utilizes the actual physical dimension of the source so that absolute intensity data can also be handled using the code. Because of this general utility, a copy of the program is included as an appendix.

CHAPTER V

EXPERIMENTAL PROCEDURES

Experimental Apparatus

R.f. power was supplied by a Radiomarine Corporation of America AN/FRT 15 radio transmitter. This transmitter was tuned to operate in the c.w. mode at 10 mc. The power was supplied to a tunable external circuit consisting of a tunable vacuum capacitor and a 5 turn, 2 inch diameter coil wound from .25 inch copper tubing. This coil generated the solenoidal field which excited the plasma. The plasma was generated in a 1.25 inch diameter, 6 inch long, quartz tube which was an appendage on a dynamically pumped vacuum chamber. The test gas was leaked into the vacuum system through a 1/8 inch Nupro shutoff valve and a 1/8 inch Nupro very fine metering valve.

This system allowed the supply gas to be shut off completely for evacuation of the system and at the same time provided fine adjustment of the operating pressure by use of the controlled leak. The external tunable circuit and the vacuum system were mounted together on a K & E instrument stand. This arrangement is shown in Figure 13. An optical system composed of a spherical front surfaced mirror and a rotating flat front surfaced mirror mounted on an optical bench was used to sweep a full-sized image of the plasma across the entrance slit of a modified Jarrell-Ash .5 m scanning monochromator.

The output of the photomultiplier tube was connected to a Tektronix 547 oscilloscope using a type 1A1 amplifier. The rotating mirror was driven by a 900 rpm synchronous motor so that the plasma (3.175 cm in diameter) was scanned in 0.7372×10^{-3} sec. This portion of the experimental apparatus is shown in Figure 14.

Power Supply

The radio transmitter was operated at 1/2 maximum plate power. By de-tuning the external circuit, a range of power inputs to the plasma could be obtained. The power to the plasma was obtained by taking the difference between the forward and backward power as measured by a Sierra Philco bi-directional power monitor and by subtracting 15 watts which went into heating the material in the neighborhood of the work coil. This power, lost to the structure, was measured by running the generator while the vacuum system was not operating. No plasma was obtained under these conditions and the power dissipated in the structure could be measured with the power meter. Since the load is considerably different with no plasma the dissipated power obtained in this manner is only an approximation so that the power inputs recorded for the various runs must be considered reasonable estimates rather than precise measurements. Subject to these limitations, low pressure plasmas were generated with input powers ranging from 220 to 740 watts.

Vacuum System

The vacuum system consisted of a 2 inch, Pyrex X-section pumped by a Welch Duo seal fore pump and a 2

inch oil diffusion pump. The diffusion pump was operated on Dow DC 704 silicon oil. Prior to a series of experimental runs, the system was evacuated to 10^{-6} mm. of mercury as recorded by an ionization gauge in the vacuum line between the diffusion pump and the chamber. After 12 hours of operation at this pressure the system was back filled with commercial grade argon (99.996% pure) through the metering system to the desired pressure, which was measured using a thermocouple gauge located in the vacuum chamber.

Spectroscopic Instrumentation

The .5 m Jarrell-Ash scanning monochromator had been previously modified to allow interchange of gratings through the use of Kelvin type mounts. Alignment and focusing of the spectrometer and the external optical system was carried out using an Optics Technology c.w. laser. The grating used in this experiment was blazed for 7500 Å and had 1180 grooves/mm which resulted in a reciprocal dispersion at the exit slit of 16 Å/mm. An EMI 9558B photomultiplier was used as the detector. For all the experimental work, the slit setting was 100 μ. Although this did not result in measurement of the total spectral line intensity, it was found that the line shapes of the lines involved were quite similar so that the ratios of the measured lines give reasonable values for total intensity ratios. The alternative to the wide slit would be a wavelength scan over the line at each spatial location and an Abel inversion for several wavelength locations near the central frequency of the line. Errors in the magnitude of the intensity ratios, due to

neglecting the local line shapes, are expected to be on the order of 5%. In view of the approximate nature of the model used, this error is not expected to be a significant limitation on the accuracy of the temperatures.

The signal output cable from the photomultiplier was shortened to 8 inches and double shielded in an attempt to reduce the r.f. noise which resulted from radiation from the work coil. In addition, the high voltage lead to the photomultiplier tube and the photomultiplier tube itself were shielded with copper. At high powers the r.f. still imposed a 10 mc harmonic on the signal which appeared to be independent of the gain on the amplifier. It was assumed that this was caused by the 10 mc signal getting to the deflection plates in the oscilloscope. This noise was tolerable however and measurements could be made. The time constant of the external circuit was not quite small enough to allow absolute following of the signal. To minimize this effect, the output data were reflected about the centerline and an average curve was used in the data analysis.

The intensity distribution across the plasma torch in a small wavelength interval was measured by sweeping a full scale image of the torch across the entrance slit of the spectrometer using the rotating mirror. Alternate sweeps were used to trigger the oscilloscope and the sweep rate of the delayed sweep was adjusted to give as large a data presentation as possible.

Data Reduction

The intensity distributions of four spectral emission lines of argon were obtained for three different input

power levels at pressures of 50 and 100 μ . The four lines used in this study consisted of the 7503.87 Å and 7514.65 Å excited atom lines and the 4806.90 Å and 4347.11 Å excited ion lines.

In addition, the intensity distributions of the 4806.90 Å and 7503.87 Å argon lines were obtained at a pressure of 1000 μ and an input power of 640 watts.

Data obtained on polaroid photographs were response corrected and plotted on graph paper. Typical response corrected data are plotted in Figures 15, 16, 17 and 18.

To get radial intensity distributions, these data were used for the numerical inversions of Abel's equation along with the code found in the appendix. Four typical radial intensity distributions are shown in Figures 19, 20, 21 and 22 which correspond to the previously mentioned response corrected data. The local values of intensity ratios at 25 radial locations for the line pairs I_{7514}/I_{4347} and I_{7503}/I_{4806} were used to obtain the temperature distributions.

CHAPTER VI

RESULTS AND CONCLUSIONS

The temperature distributions in the discharge as determined from the line ratios I_{7514}/I_{4347} and I_{7503}/I_{4806} are plotted in Figures 23 through 29. All of the temperature distributions have essentially the same scatter as well as the same general shape. The distributions determined using the ratio I_{7503}/I_{4806} all exhibit an inflection point approximately midway between the axis and the wall. This was probably due to error introduced in the inversion of Abel's equation which causes some scatter near sharp peaks in the inverted data.

The temperature distributions obtained exhibited maximum temperatures on the axis of symmetry of the discharge. The magnitude of this on-axis-peak is in exceptionally good agreement with the asymmetric double probe data of Keefer, et al.[14] Averaged, on-axis temperatures are presented in Table 1. It can be seen on Figure 23 that the temperature drops from this on-axis maximum to approximately 85% of the axial value at a distance of 2/3 of the radius. No behavior of this nature has been observed with the probes. Referring to Figure 30 it may be seen that the temperature is a rather weak function of the input power in the power range of 220 to 740 watts. This particular behavior has not been observed with probe techniques. It would seem that the spectro-

metric technique is more sensitive to electron temperature variations than the probe techniques. In view of the approximate nature of the plasma model used, the absolute magnitude of the measured temperatures is subject to some question. However, the general agreement between the probe and spectrometric techniques tends to verify the model. Presumably, errors in calculating the excited state populations in the successive ionization stages tend to cancel when a ratio is taken.

A calculation of the ratio of number density of ArIII to ArII using equation (2.21), an assumed electron number density of 10^{12} cm^{-3}, and a temperature of 1.5 ev. yields a number of the order 10^{-5}. Assuming the plasma to be quasi-neutral and neglecting double ionization Dalton's law may be applied to the plasma. For an assumed neutral gas and in temperature of 0.2 ev. the electron number density is approximately 5×10^{13} cm^{-3} for a total pressure of 100 microns. In view of the approximations made in applying Dalton's law and the approximate nature of the plasma model this must be considered an order of magnitude estimate for the axial value of the number density. No attempt was made to converge on a self-consistent temperature and electron number density since the measured temperatures are only slightly influenced by the electron number density and absolute magnitude of the number density would remain subject to the assumed ion and neutral temperature.

The electron number density could also be inferred from the absolute intensity of an ion emission line. However, this requires an accurate value for the population density of the higher excited state, which the

approximate model used probably does not provide.

In the type of discharge studied, it is probable that diffusive loss of ions to the wall is a significant loss mechanism. At the present time there does not appear to be an approximate semi-corona model which will suit such a loss mechanism. If a solution of the rate equations for argon were possible this loss mechanism could be accounted for. This seems to be impossible in the near future. It is suggested that future work on the electrodeless discharge should utilize hydrogen or helium. The theory for hydrogenic ions could then be applied, including the diffusive loss to the walls.

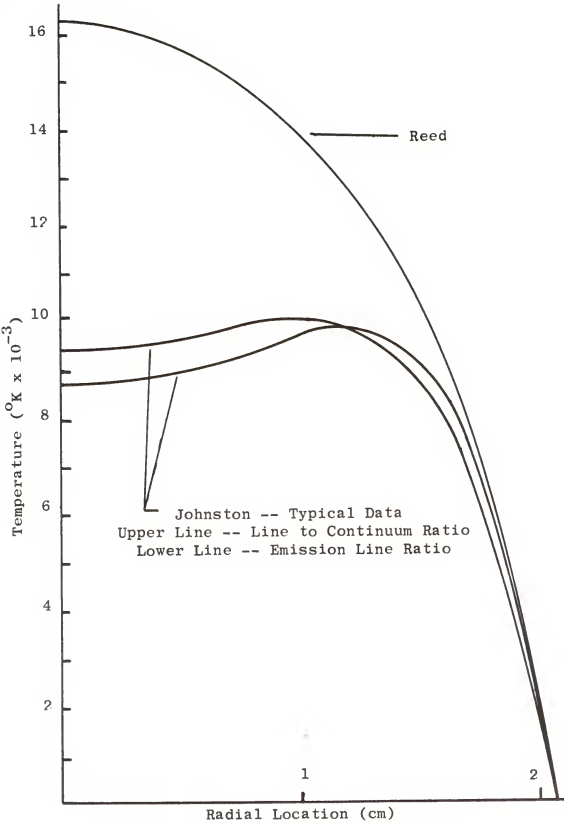

Figure 1 Temperature Distribution.

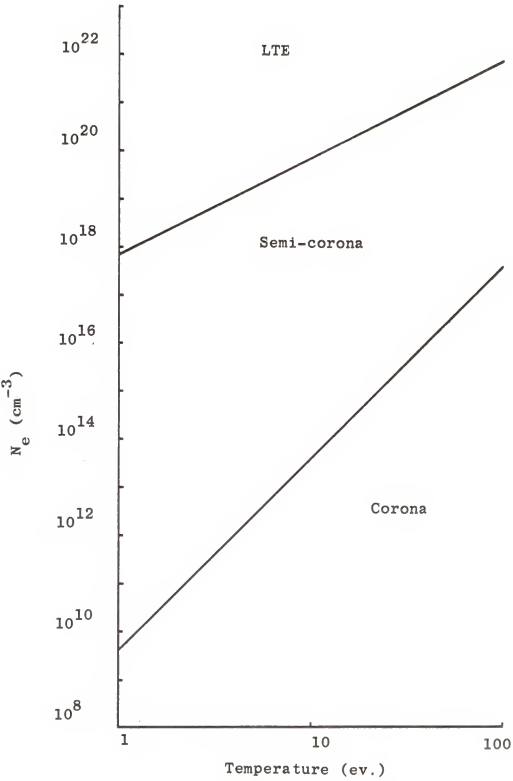

Figure 2 Domains of Validity for an Optically Thin Argon Plasma.

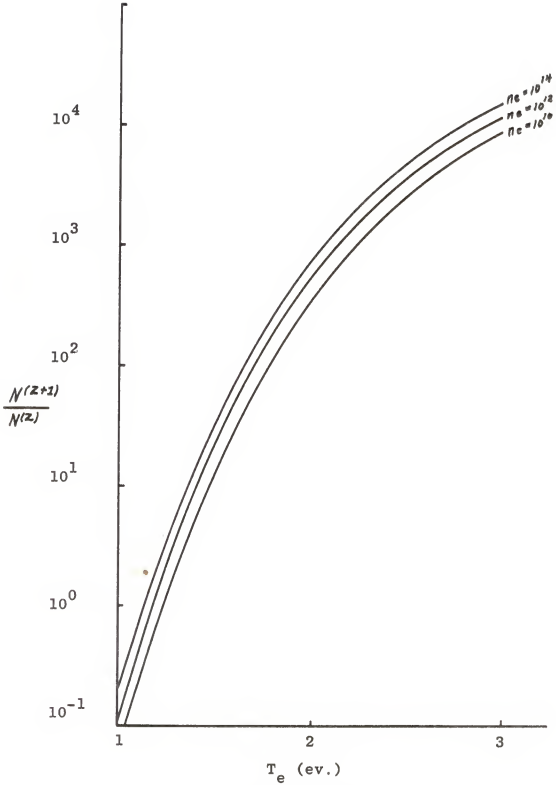

Figure 3 Ratio of Neutral Atoms to Singly Ionized Ions for Argon.

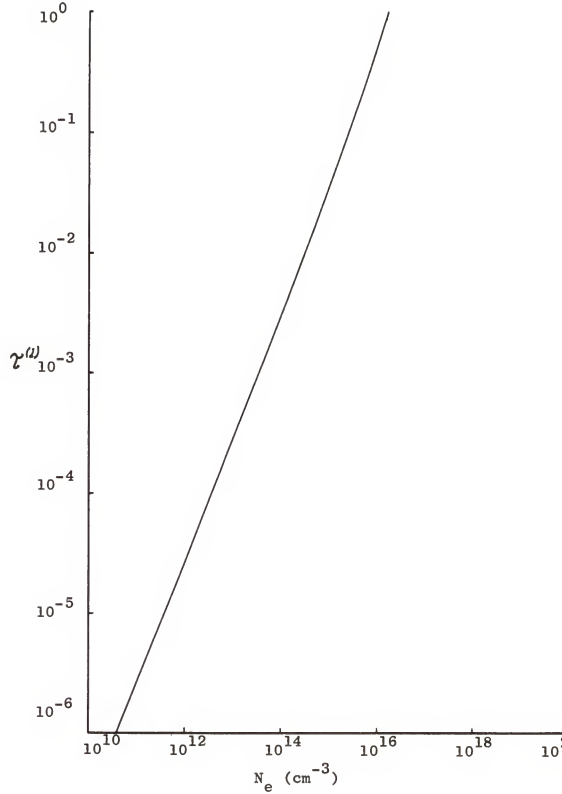

Figure 4 Saha Equation Correction Factor for Argon Atoms.

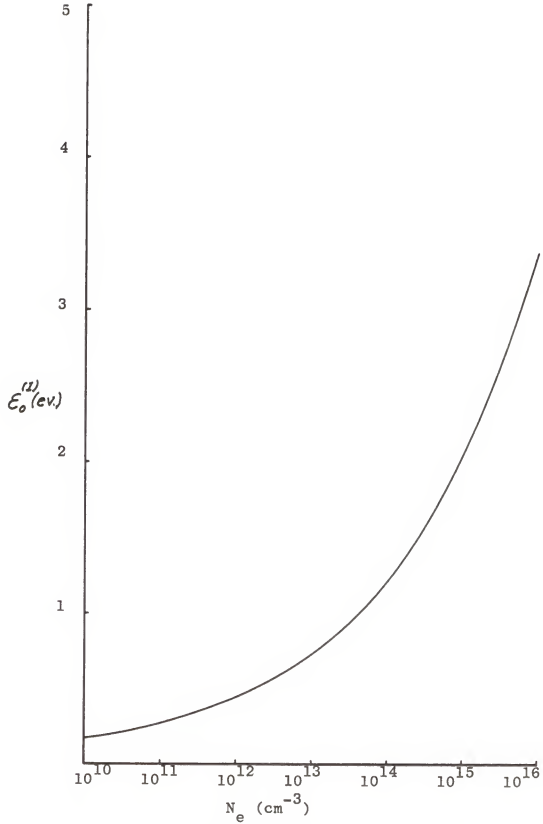

Figure 5 Collision Limit for Argon Atoms.

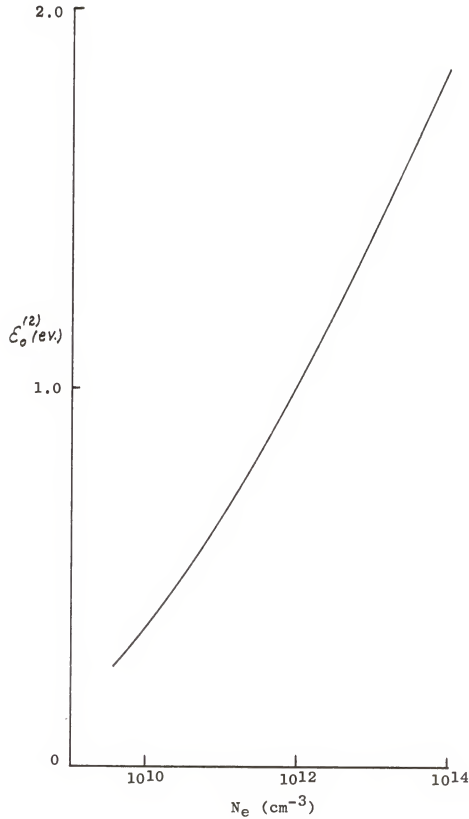

Figure 6 Collision Limit for Argon Ions.

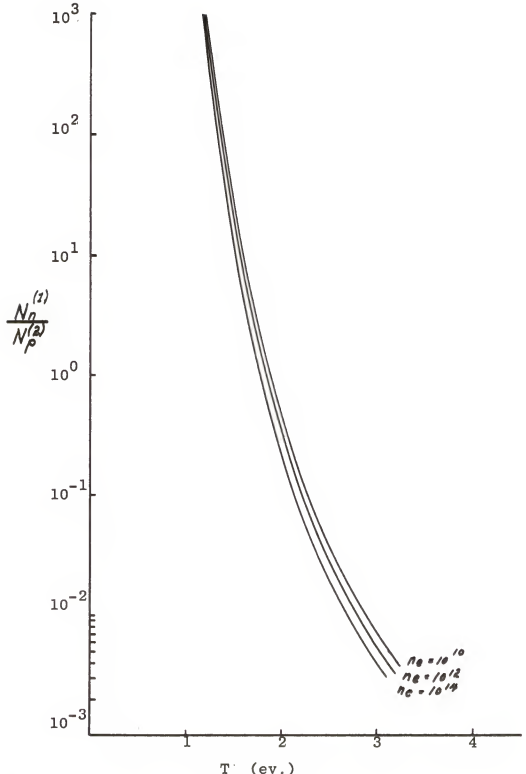

Figure 7 Ratio of Excited Neutrals to Excited Ions.

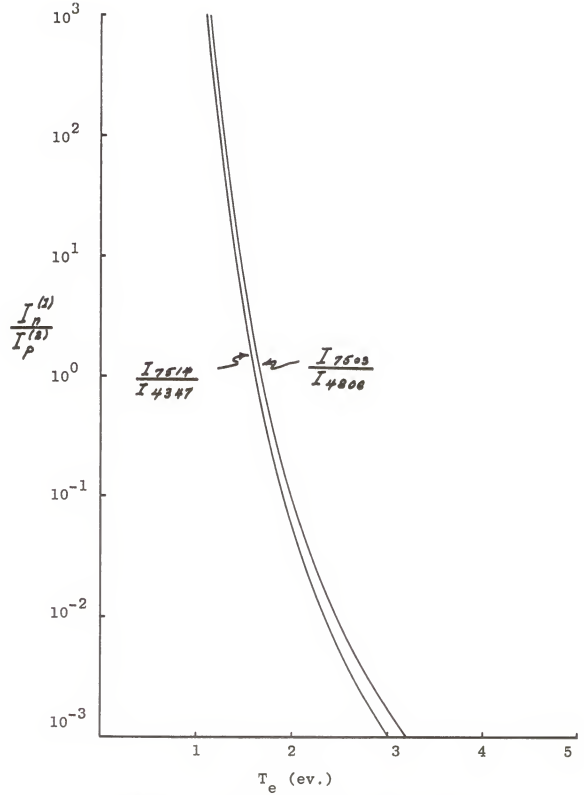

Figure 8 Emission Line Intensity Ratio.

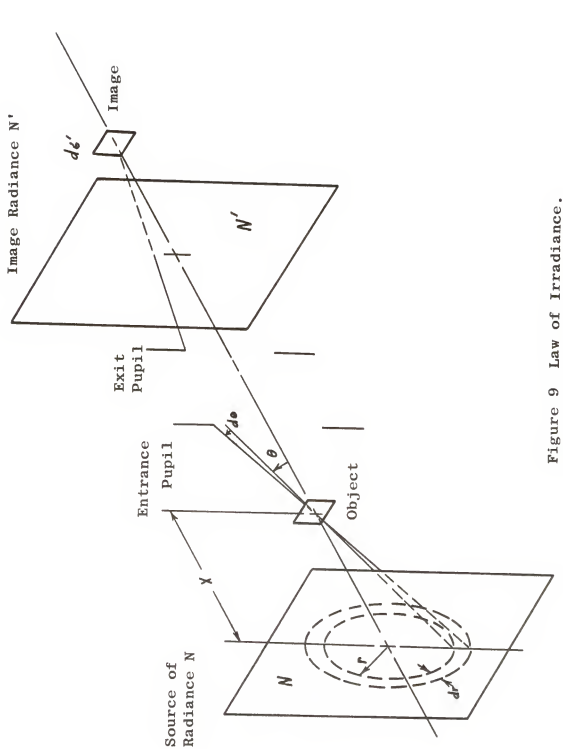

Figure 9 Law of Irradiance.

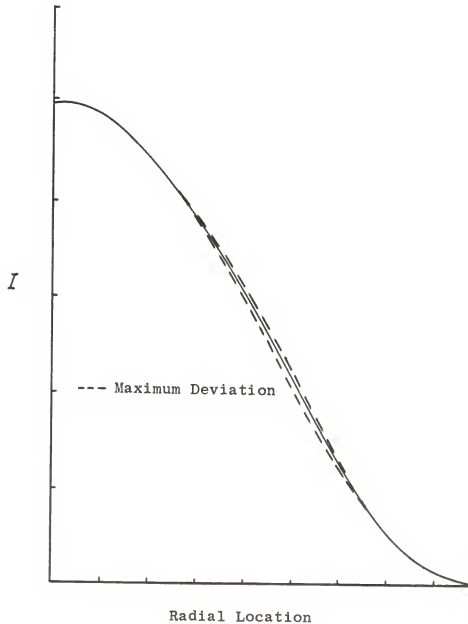

Figure 10 Experimental Verification of the Law of Irradiance.

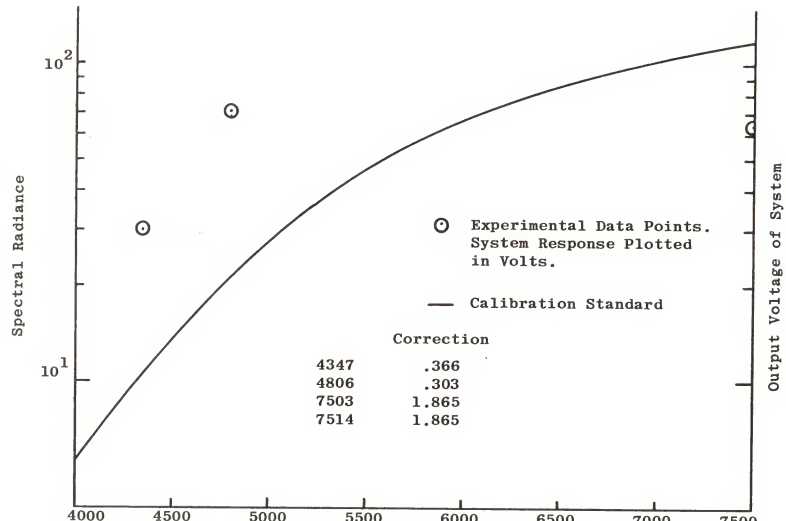

Figure 11 Spectral Intensity Calibration.

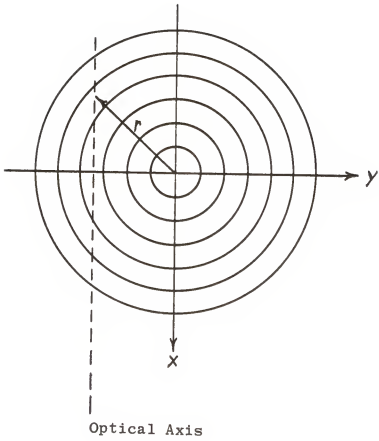

Figure 12 Geometry of the Source.

Figure 13 Plasma Chamber.

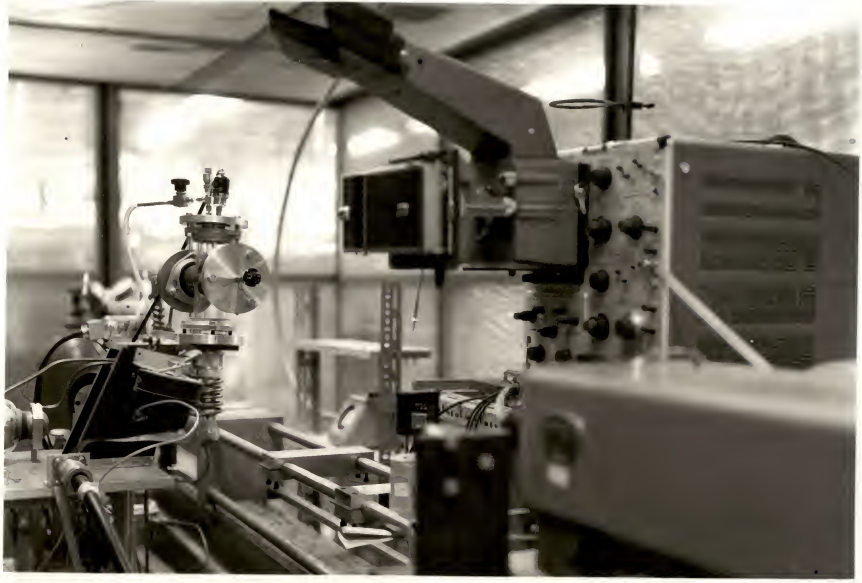

Figure 14 Instrumentation.

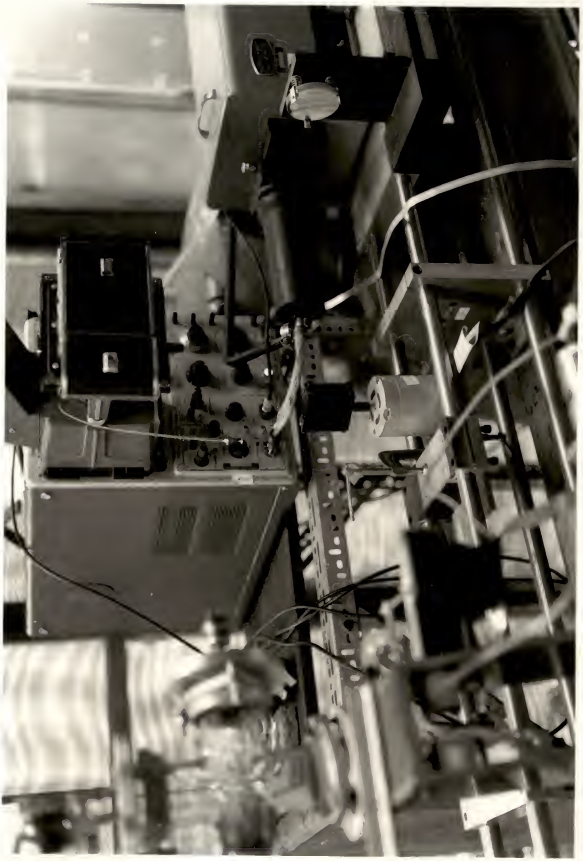

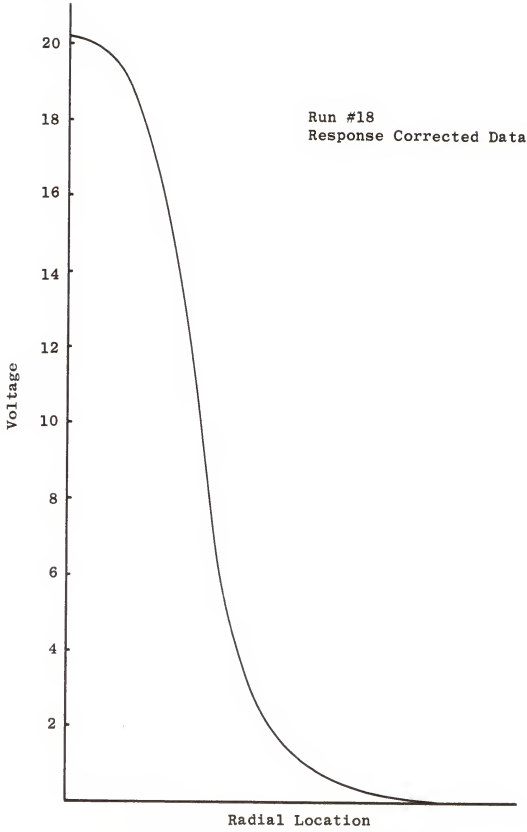

Figure 15 Integrated Intensity Profile 4806 Å.

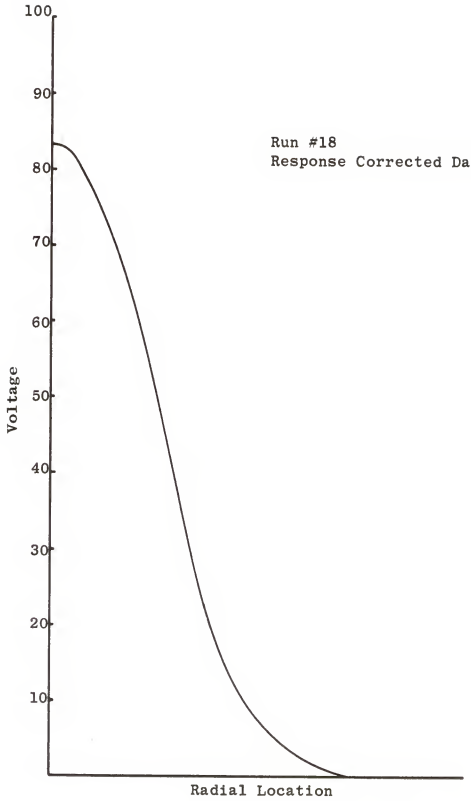

Figure 16 Integrated Intensity Profile 4347 Å.

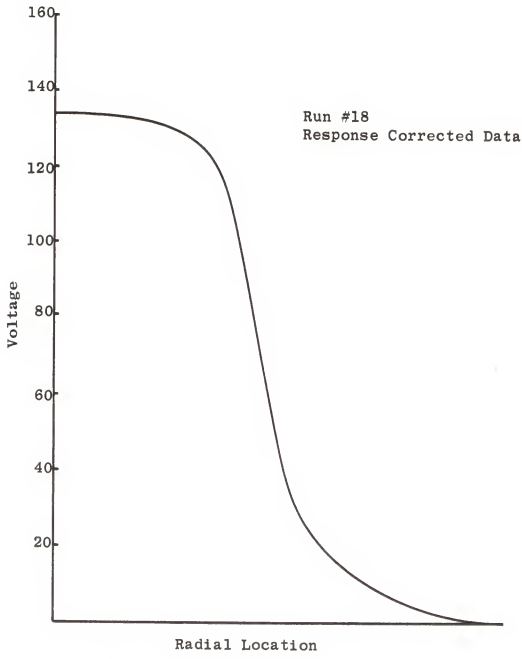

Figure 17 Integrated Intensity Profile 7503 Å.

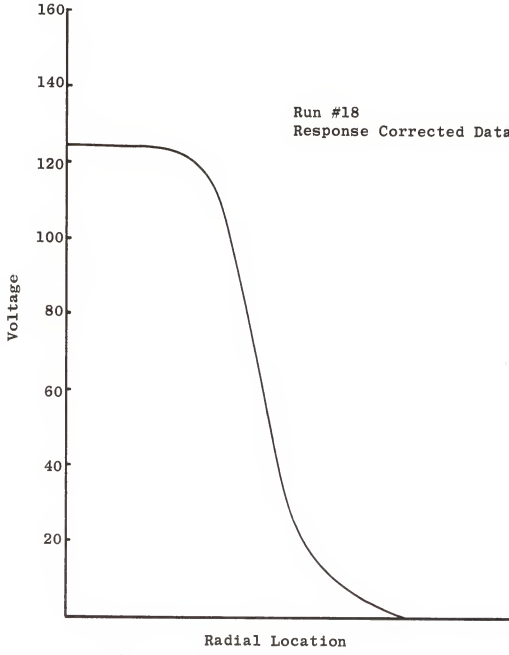

Figure 18 Integrated Intensity Profile 7514 Å.

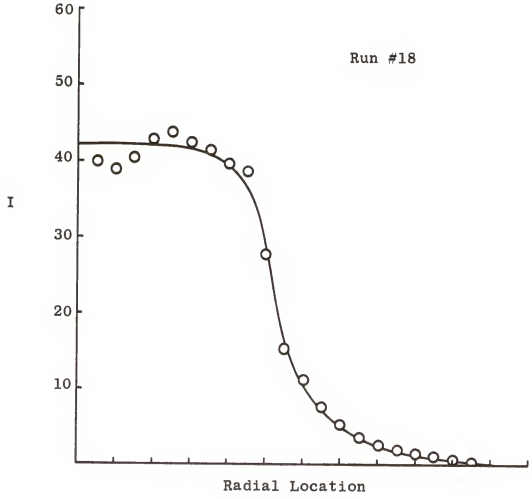

Figure 19 Radial Intensity Distribution 4806 Å.

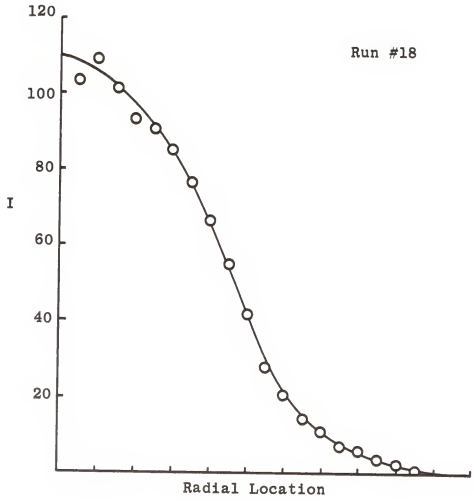

Figure 20 Radial Intensity Distribution 4347 Å.

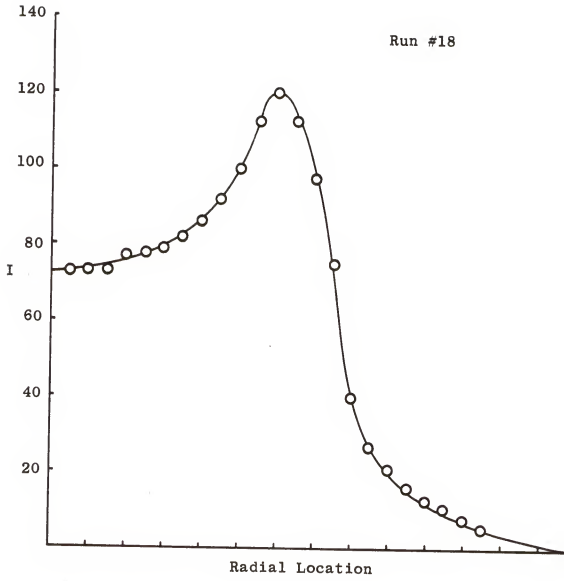

Figure 21 Radial Intensity Distribution 7503 Å.

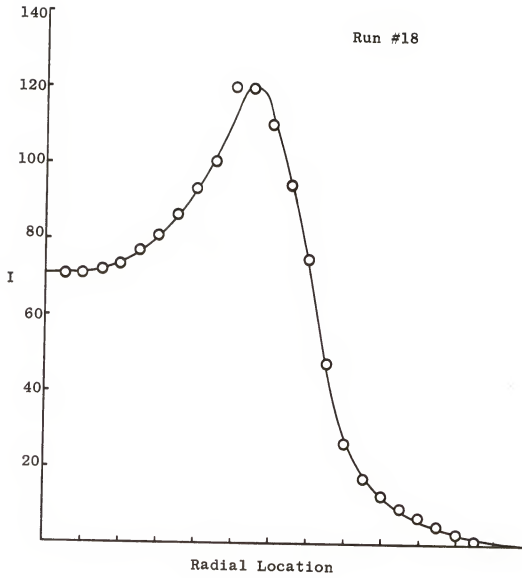

Figure 22 Radial Intensity Distribution 7514 Å.

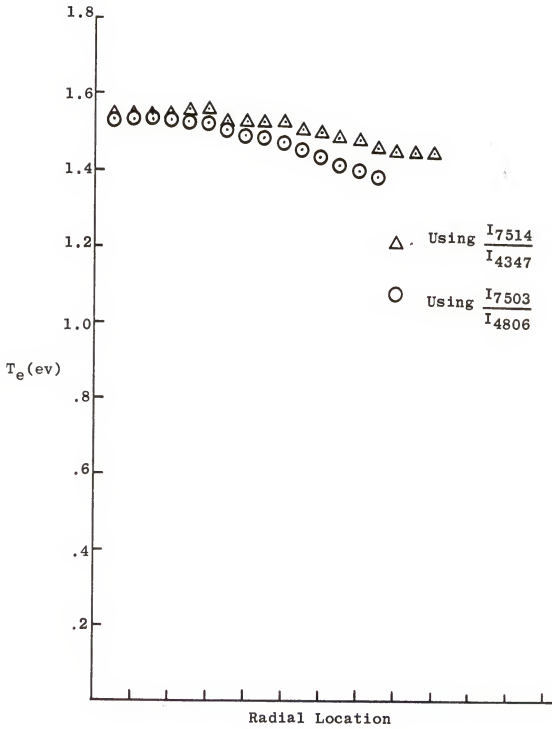

Figure 23 Radial Temperature Distribution Run 13.

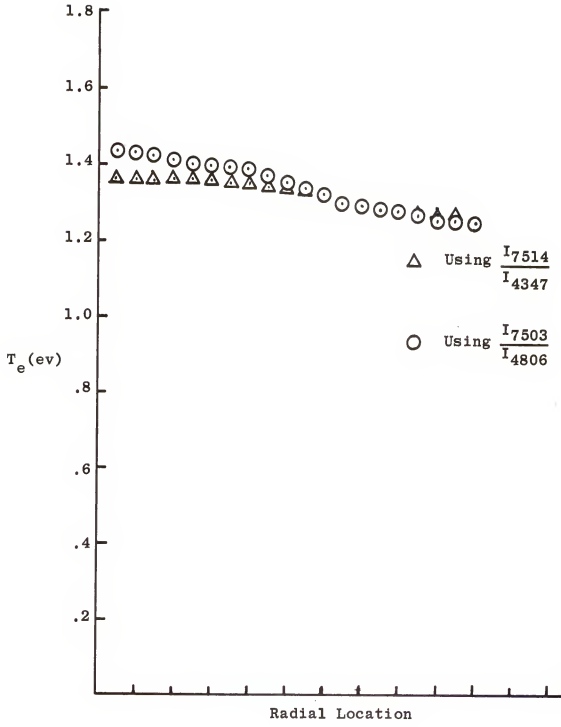

Figure 24 Radial Temperature Distribution Run 14.

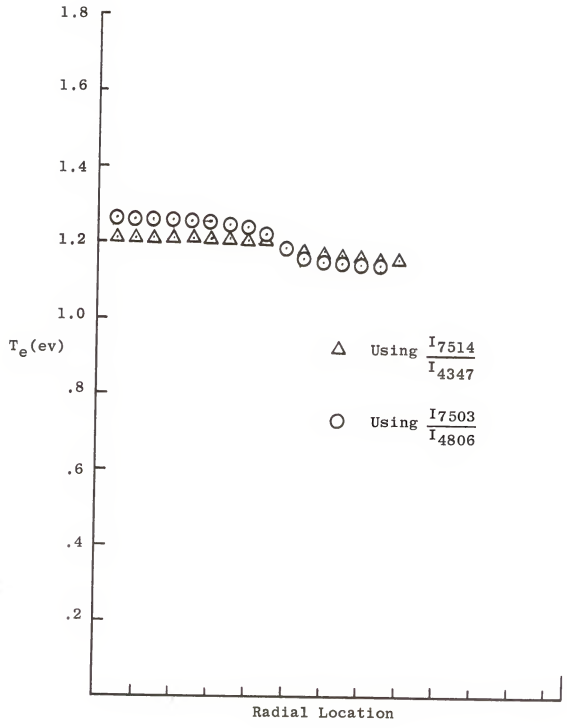

Figure 25 Radial Temperature Distribution Run 15.

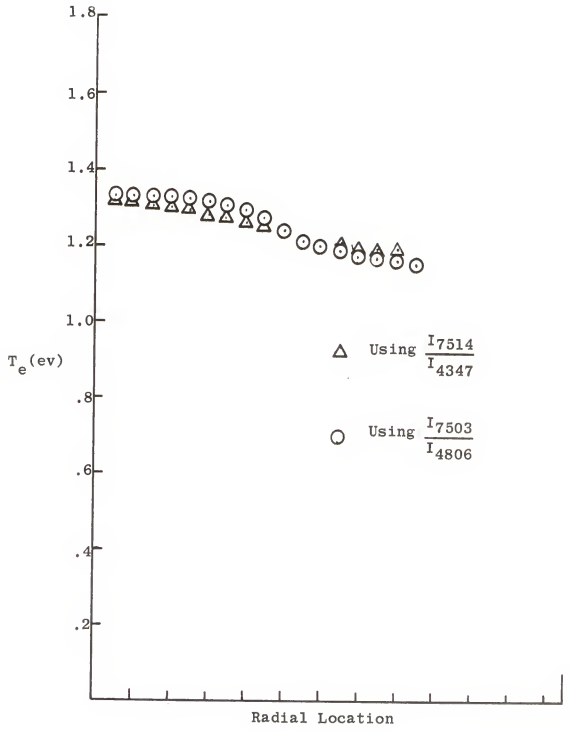

Figure 26 Radial Temperature Distribution Run 16.

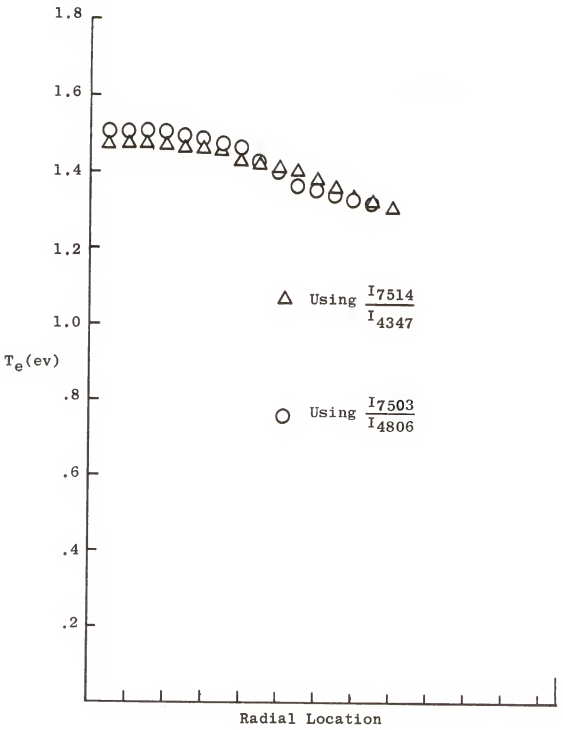

Figure 27 Radial Temperature Distribution Run 17.

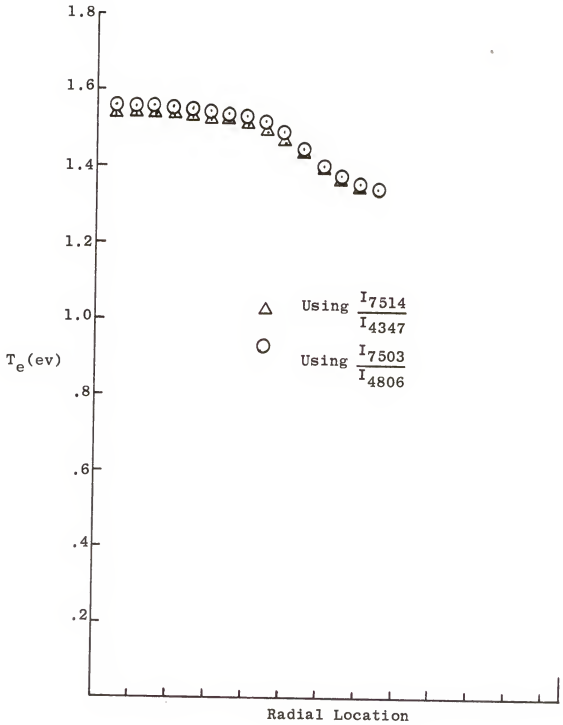

Figure 28 Radial Temperature Distribution Run 18.

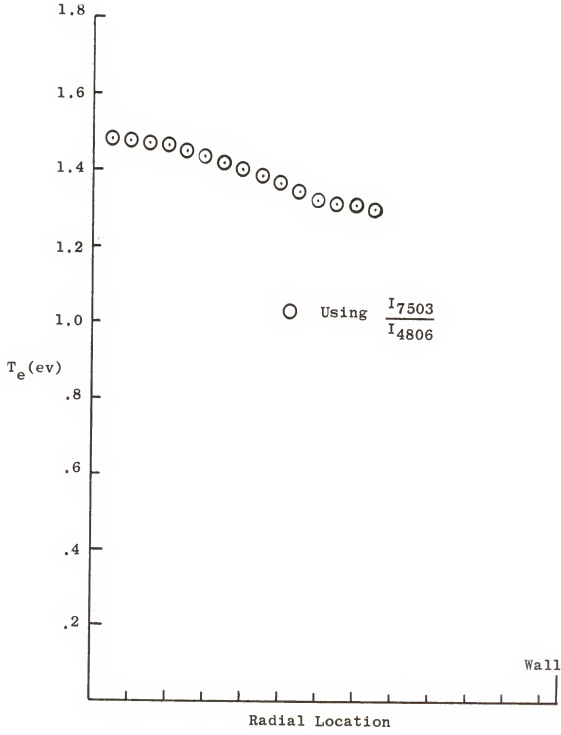

Figure 29 Radial Temperature Distribution Run 19.

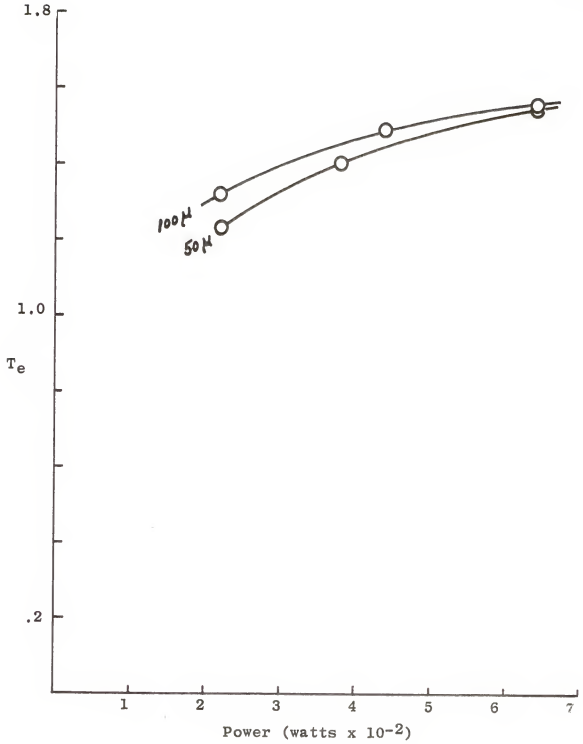

Figure 30 Peak Temperature as a Function of Input Power.

Table 1

Results

Run No.	Temperature (ev)		Pressure Microns of Hg	Input Power Watts
	$\frac{I_{7514}}{I_{4347}}$	$\frac{I_{7503}}{I_{4806}}$		
13	1.55	1.53	50	640
14	1.36	1.43	50	380
15	1.21	1.26	50	220
16	1.31	1.33	100	220
17	1.47	1.50	100	440
18	1.56	1.53	100	740
19		1.48	1000	640

APPENDIX

NUMERICAL INVERSION OF ABEL'S EQUATION

The data input for the following Fortran IV program consists of one card, using format 1, with the length of the source radius in arbitrary units, followed by as many sets of 4 cards, using format 3, as there are data to be processed. These 4 card sets contain the integrated intensity data for 25 radial locations.

```
C       PROGRAM TO CALCULATE DISTANCE FROM THE OBJECT PLANE
        SOURCE DIVIDED INTO 25 CONCENTRIC RINGS
      1 FORMAT (1F10.5)
      2 FORMAT (3X,26HDISTANCE FROM OBJECT PLANE)
      3 FORMAT (7F10.5)
      4 FORMAT (3F10.6)
      5 FORMAT  ( 5X, 23HDEFOCUSING COEFFICIENTS, 3X, (3F10.6) )
      6 FORMAT (10F10.5)
     12 FORMAT (1X,30HDEFOCUSING COEFFICIENTS S(K,J) )
        DIMENSION A(26,26), RA(25), R(25),G(25,25),
        E(25,25),S(25,25)
        DIMENSION B(26,25), Y(25), X(26), Z(25), V(26,26)
    139 READ (5,1) RAD
         DO 7 K = 1,25
         DO 7 J = 1,K
        RA(K) = (RAD/25.0)*FLOAT(K)
        R(J) = (RAD/25.0)*FLOAT (J) - ( (RAD/25.0)*2.0 -
        (RAD/25.0) )*0.5
        A(K,J) = (RA(K)**2.0 - R(J)**2.0)**0.5
      7 CONTINUE
        WRITE (6,2)
        WRITE (6,3)        ( (A(K,J),J=1,K),K=1,25)
C        PROGRAM TO CALCULATE LENGTH COEFFICIENTS FOR
         ABELS EQUATION
     15 FORMAT(1X,19HLENGTH COEFFICIENTS)
        DO 120 K = 2,26
        L = K -1
        DO 120 J = 1,L
```

```
  120  V(K,J) = A(L,J)
       DO 125 J = 1,25
  125  V(J,J) = 0.0
       DO 130 K = 1,25
       DO 130 J = 1,K
        L = K + 1
  130  B(K,J) = (V(L,J) - V(K,J) )* 2.0
       WRITE (6,15)
       WRITE (6,6)          ( (B(K,J),J = 1,K),K = 1,25)
C       INVERSION OF ABELS EQUATION - 25 RINGS, Y -
        EXPERIMENTAL DATA
   13   FORMAT (1X, 15HINPUT INTENSITY)
   14  FORMAT(1X, 16HOUTPUT INTENSITY)
  131  READ (5,3)            (Y(I),I = 1,25)
        DO 150 K = 1,25
        I = 26 - K
        X(26) = 0.0
        J = I
        Z(I) = 0.0
  140  Z(I) = Z(I) + X(J+1)*B(J+1,I)
        IF (25-J)150,150,145
  145  J = J+1
        GO TO 140
  150  X(I) = (Y(I) - Z(I) )/(B(I,I) )
       CONTINUE
       WRITE (6,13)
       WRITE (6,6) (Y(I), I=1,25)
       WRITE (6,14)
       WRITE (6,6)          (X(I), I = 1,25)
         GO TO 131
       END
```

LIST OF REFERENCES

1. Hittorf, W., "Ueber die Electricitätsleitung der Gase," Wied. Ann. Phys. Chim., 21, 90 (1884).

2. Thomson, J. J., "The Electrodeless Discharge through Gases," Phil. Mag., 4, 1128-1160 (1927).

3. Townsend, J. S. and Donaldson, R. H., "Electrodeless Discharges," Phil. Mag., 5, 178-191 (1928).

4. Lehrmann, O., "Ueber das Entladungspotentialgefälle," Wied. Ann. Phys. Chim., xdvii, 42 (1892).

5. MacKinnon, K. A., "On the Origin of the Electrodeless Discharge," Phil. Mag., 7, 8, 52, 605 (1929).

6. Reed, T. B., "Induction-Coupled Plasma Torch," J. Appl. Phys., 32, 5, 821 (1961).

7. Reed, T. B., "High Power Low-Density Induction Plasmas," J. Appl. Phys., 34, 10, 3146 (1963).

8. Pell, K. M., "Diagnostics of an RF Plasma Based on Heat Transfer Rates," Thesis, Univ. of Fla. (1963).

9. Gold'farb, V. M., and Dresvin, S. V., "Optical Investigation of the Distribution of Temperature and Electron Concentration in an Argon Plasma," Teplofizika Vysokikh Temperatur, 3, 333 (1965).

10. Pettit, W. T., "Temperature Distribution in an RF Discharge Determined from the Absolute Intensity of Radiation," Thesis, Univ. of Fla. (1966).

11. Johnston, P. D., "Temperature and Electron Density Measurements in an RF Discharge in Argon," Phys. Lett., 20, 5, 499 (1966).

12. Clarkson, M. H., Field, R. E., and Keefer, D. R., "Electron Temperatures in Several rf-Generated Plasmas," AIAA Jour., 4, 3, 546 (1966).

13. Keefer, D. R., Clarkson, M. H., and Mathews, B. E., "Probe Measurements in an Electrodeless Discharge," AIAA Jour., 4, 10, 1858 (1966).

14. Porter, R. F., "A Spectrometric Investigation of Low Pressure R.F. Plasmas," Thesis, Univ. of Fla. (1967).

15. Sovie, R. J., "Spectroscopic Determination of Electron Temperature and Percentage Ionization in a Helium Plasma," Phys. Fluids, 7, 613 (1964).

16. Sovie, R. J., Private Communication, Oct. (1966).

17. Oertel, G. K. and Griem, H. R., "Spectral Line Emission from a Transient Nonuniform Plasma," Phys. of Fluids, 8, 1 (1966).

18. McWhirter, R. W. P., Plasma Diagnostic Techniques, ed. Huddlestone and Leonard, Academic Press, N.Y., 1965.

19. Schneider, R. T., and Oertel, G. K., Unpublished Manuscript.

20. Bates, D. R., Kingston, A. E., and McWhirter, R. W. P., "Recombination between electrons and atomic ions. I Optically thin plasmas," Proc. Roy. Soc., A267, 297 (1962).

21. Griem, H. R., Plasma Spectroscopy, McGraw Hill, N.Y., 1965.

22. Schneider, R. T., Private Communication. (1966).

23. Wilson, R., "The Spectroscopy of Non-Thermal Plasmas," J. Quant. Spectrosc. Radiat. Transfer, 2, 477 (1962).

24. Olsen, H. N., "The Electric Arc as a Light Source for Quantitative Spectroscopy," J. Quant. Spectrosc. Radiat. Transfer, 3, 305 (1963).

25. Pearce, W. J., Conference on Extremely High Temperatures, ed. Fischer and Mansur, John Wiley & Sons, Inc., N.Y., 1958.

BIOGRAPHICAL SKETCH

Kynric Martin Pell was born April 5, 1938, at Toronto, Ontario, Canada. He attended Runnymede Collegiate Institute in Toronto until June, 1956. Following a move to Florida, he received the degree Associate of Arts from Palm Beach Junior College in June, 1959. From 1959 until 1962, he attended the University of Florida, receiving the degree Bachelor of Aerospace Engineering in June, 1962. In the spring of 1962 he obtained his United States Citizenship in Naturalization proceedings in Miami, Florida. The summer of 1962 he was employed as an Analytical Design Engineer with Pratt and Whitney Aircraft, East Hartford, Connecticut. After enrolling in the Graduate School of the University of Florida in the fall of 1962 he obtained the degree Master of Science in Engineering in December, 1963.

In January, 1964, Mr. Pell was appointed Research Associate in the Department of Aerospace Engineering. From that time to the present he has pursued the degree Doctor of Philosophy in the Department of Aerospace Engineering.

Kynric Martin Pell is married to the former Ann Louise Brenn. They are the parents of two children, Kymberly Michelle, and Kynric, Jr. Mr. Pell is an associate member of the American Institute of Aeronautics and Astronautics.

This dissertation was prepared under the direction of the chairman of the candidate's supervisory committee and has been approved by all members of that committee. It was submitted to the Dean of the College of Engineering and to the Graduate Council, and was approved as partial fulfillment of the requirements for the degree of Doctor of Philosophy.

August, 1967

Dean, College of Engineering

Dean, Graduate School

Supervisory Committee:

Chairman